NASA TECHNICAL MEMORANDUM

NASA TM-73,246

NASA TM-73,246

INFLUENCE OF TEMPERATURE AND THE ROLE OF CHROMIUM ON THE KINETICS OF SULFIDATION OF 310 STAINLESS STEEL

D. Bhogeswara Rao
Ames Research Center, Moffett Field, California 94035 and
Department of Materials Science and Engineering
University of California, Berkeley, California 94720

and

Howard G. Nelson
Ames Research Center
Moffett Field, California 94035

March 1977

1. Report No.	2. Government Accession No.	3. Recipient's Catalog No.
NASA TM-73,246		

4. Title and Subtitle	5. Report Date
INFLUENCE OF TEMPERATURE AND THE ROLE OF CHROMIUM ON THE KINETICS OF SULFIDATION OF 310 STAINLESS STEEL	6. Performing Organization Code

7. Author(s)	8. Performing Organization Report No.
D. Bhogeswara Rao* and Howard G. Nelson**	A-7058
	10. Work Unit No. 778-11-02
9. Performing Organization Name and Address	11. Contract or Grant No.
*Ames Research Center, NASA, Moffett Field, California 94035 and Department of Materials Science and Engineering University of California, Berkeley, California 94720 **Ames Research Center, NASA, Moffett Field, California 94035	13. Type of Report and Period Covered Technical Memorandum
12. Sponsoring Agency Name and Address	14. Sponsoring Agency Code
National Space and Aeronautics Administration Washington, D. C. 20546	

15. Supplementary Notes

16. Abstract

The sulfidation of 310 stainless steel was studied over the temperature range from 910 K to 1285 K. By adjusting the ratio of hydrogen to hydrogen sulfide, variations in sulfur potential were obtained. The effect of temperature on sulfidation was determined at three different sulfur potentials: 39 Nm^{-2}, 1.4×10^{-2} Nm^{-2}, and 1.5×10^{-4} Nm^{-2}. All sulfide scales contained one or two surface layers in addition to a subscale. The second outer layer (OL-II), furthest from the alloy, contained primarily Fe-Ni-S. The first outer layer (OL-I), nearest the subscale, contained Fe-Cr-S. The subscale consisted of sulfide inclusions in the metal matrix. At a given temperature and sulfur potential, the weight gain data obeyed the parabolic rate law after an initial transient period. The parabolic rate constants obtained at the sulfur potential of 39 Nm^{-2} did not show a break when the logarithm of the rate constant was plotted as a function of the inverse of absolute temperature. Sulfidation carried out at sulfur potentials below 2×10^{-2} Nm^{-2}, however, did show a break at 1145 K which is termed as the transition temperature. This break was found to be associated with the changes which had occurred in the Fe:Cr ratio of OL-I. Below the transition temperature the activation energy was found to be approximately 125 kJ $mole^{-1}$. Above the transition temperature the rate of sulfidation decreased with temperature but dependent on the Fe:Cr ratio in the iron-chromium-sulfide layers of the OL-I. A reaction mechanism consistent with the experimental results has been proposed.

17. Key Words (Suggested by Author(s))	18. Distribution Statement
Sulfidation of 310 stainless steel Sulfidation kinetics Temperature dependence Sulfide scale morphology Reaction mechanism	Unlimited STAR Category – 23

19. Security Classif. (of this report)	20. Security Classif. (of this page)	21. No. of Pages	22. Price*
Unclassified	Unclassified	40	$3.75

*For sale by the National Technical Information Service, Springfield, Virginia 22161

Influence of Temperature and the Role of Chromium on the Kinetics of Sulfidation of 310 Stainless Steel

D. Bhogeswara Rao* and Howard G. Nelson**

KEY WORDS: Sulfidation of 310 Stainless Steel; sulfidation kinetics; temperature dependence; sulfide scale morphology; reaction mechanism.

---

*Materials and Physical Sciences Research Branch, NASA-Ames Research Center, Moffett Field, CA 94035 and Department of Materials Science & Engineering, University of California, Berkeley, CA 94720.

**Materials and Physical Sciences Research Branch, NASA-Ames Research Center, Moffett Field, CA 94035

INTRODUCTION

Corrosion studies at high temperatures on structural engineering materials in sulfur containing gases are of considerable industrial importance. Sulfur is an unavoidable contaminant in hot combustion atmospheres derived from coals and other fuels. The present day interests in the coal conversion systems require corrosion data for commercial alloys in sulfur containing gases. One of the candidate materials for the fabrication of the internal components of coal gasifiers is SAE 310 stainless steel. It was, therefore, decided to study the sulfidation problems associated with the austenitic stainless steel over a broad range of sulfur potentials and temperatures, as a part of the continuing program on the corrosion of internal components of coal gasifiers. The specific influence of sulfur potential on the sulfidation of SAE 310 stainless steel, at an isothermal temperature of 1065 K, has been reported in a previous publication.[1] The present article deals with the influence of temperature on the kinetics of sulfide scale formation and the composition and morphology of the associated scaling layers. The specific role of Cr and the lesser roles of Fe and Ni on the rate of sulfidation of austenitic stainless steel has also been discussed in some detail.

MATERIALS AND PROCEDURES

Test coupons 2 cm by 1.25 cm by 0.33 cm were prepared from a commercially produced cold-rolled, SAE 310 stainless steel. The composition of this alloy and the sample preparation procedures were given in an earlier publication.[1] Coupon dimensions were measured to an accuracy of 0.001 cm by use of a micrometer, and the surface area was calculated.

Commercially available high-purity hydrogen and hydrogen sulfide gases were used and were further purified by passing them through a purification train designed to remove residual water vapor and oxygen. Gas flow rates were monitored and controlled by electronic mass flow controllers. The sulfur potential of a run was calculated from the ratio of hydrogen to hydrogen sulfide using the equilibrium relationship

$$H_2S(g) \rightleftharpoons H_2(g) + 1/2\ S_2(g) \qquad (1)$$

where the dimeric sulfur is the predominant species. The free energy functions for these calculations were taken from the 'JANAF' thermochemical tables.[2]

Sulfidation kinetics were measured using the weight gain technique. Weight change was continuously monitored to a sensitivity of 0.1 mg employing an 'AINSWORTH' analytical thermobalance. The balance system was purged with argon to avoid condensation of sulfur and any reaction with the balance components. At the same time, sufficient precautions were taken not to dilute the test gas mixture. A recrystallized alumina tube, 5 cm in diameter, served as a reaction chamber. The chamber was connected to the balance unit by means of a gastight, 'O'-ring seal. The reaction chamber was surrounded by a resistance furnace. Furnace temperature control was achieved by a potentiometric controller in conjunction with a chromel-alumel thermocouple positioned close to the furnace windings. Temperature was found to be uniform within ±1°C over the middle 5 cm of the reaction chamber. The actual coupon temperature was estimated by means of two Pt-Pt (10%Rh) thermocouples located near both ends of the coupon. It is estimated that coupon temperature was kept constant to within ±3°C during any run.

The test coupon, suspended from one arm of the balance by an alumina-sheathed platinum wire, was lowered into the constant temperature zone of the reaction chamber. At the higher sulfur pressures, where some reaction with platinum was noticed, a gold wire was used. The coupon was brought to the desired temperature under a vacuum of better than 10^{-4} Nm^{-2}. Argon was then passed through the balance assembly, and, at the same time, hydrogen was passed through the reaction chamber to reduce any oxide traces that may have formed during handling of the coupon. The reaction gases, at the desired ratio of hydrogen to hydrogen sulfide, were allowed to mix in a mixing chamber. The experiment was initiated at the moment the reactive gas mixture was allowed to pass through the reaction chamber. During all experiments, a constant reactive gas flow rate of 500 cc min^{-1} or greater was maintained. At the end of each run the flow of reactive gas was halted and argon flow was resumed while the coupon was being cooled. When the system had attained room temperature, the coupon was removed and the corrosion product was examined. The continuously recorded weight gain data were converted to weight gain per unit area and used to calculate the appropriate rate equations. Additionally, some test samples were quenched from the reaction temperature in order to facilitate the identification of sulfide phases that were formed at the reaction temperature and to avoid disproportionation of reaction products on cooling.

At the end of an experiment the coupon was sectioned with a diamond saw, mounted, polished, and examined using metallographic techniques. In order to resolve the finer details of the microstructures of reaction products, the polished cross section of the reacted samples were also examined by scanning electron microscopy. In many cases, the scales flaked off during cooling; such scales were collected and examined separately from the unreacted alloy.

The morphology and the composition of the scales were examined using scanning electron microscopy, energy dispersive X-ray analysis and electron microprobe analysis. To permit quantitative analysis, FeS_2 was used as a sulfur standard and the SAE 310 stainless steel was used as a standard for Fe, Ni and Cr. In all cases, atomic absorption and fluorescence effects were eliminated using appropriate computer programs.

The sulfide phases present in these scales were identified using X-ray diffraction techniques. Because of the complex nature of the scaling layers, it was only possible to identify the major phases present by this technique. More accurate and detailed analysis was possible by the critical examination of the microstructure of the scales and by compositional analysis of different phases using both energy dispersive X-ray and electron microprobe analysis. In a scaling layer conglomerate of different phases, the relative amount of each phase was determined employing "QUANTIMET 700". This technique was particularly useful in determining the eutectic compositions.

RESULTS

Reaction Kinetics

Sulfidation kinetics of SAE 310 stainless steel was studied as a function of temperature at three different sulfur potentials, 39 Nm^{-2} (3.69×10^{-4} atm), 1.4×10^{-2} Nm^{-2} (1.3×10^{-7} atm) and 1.5×10^{-4} Nm^{-2} (1.42×10^{-9} atm) over the temperature range from 910 K to 1285 K. Weight gain data obtained at these three sulfur potentials are shown in Figs. 1, 2 and 3, respectively. All data are plotted according to the parabolic equation;

$$(\Delta W/A)^2 = K_p'' \, t \qquad (2)$$

As seen in Fig. 1, at a sulfur potential of 39 Nm^{-2}, the reaction obeys the parabolic relationship with the exception of a transient period at the very early stages of sulfidation. A decrease in this transient period with increasing temperature is seen to occur. An analysis of the slopes of the linear portion of the curves gives the parabolic rate constants, K_p''. The logarithm of these parabolic rate constants as a function of the reciprocal of the absolute temperature is shown as the upper curve in Fig. 4 and yields an activation energy of 121 ± 8 kJ $mole^{-1}$. Due to very rapid increase in reaction rate with temperature, a 0.5 mm scale developed in less than 50 minutes at the higher temperatures.

The data obtained at the sulfur potentials of 1.4×10^{-2} Nm^{-2} and 1.5×10^{-4} Nm^{-2} are shown in Figs. 2 and 3, respectively. The data at the intermediate sulfur potential (Fig. 2) is seen to differ from that obtained at the higher potential (Fig. 1) in two ways. Although the transient period still decreases with increasing temperature, in general it is increased compared with that observed at 39 Nm^{-2} (Fig. 1). Additionally, the rate of sulfidation is seen to increase progressively with temperature up to 1145 K and then suddenly decrease with a further increase in temperature. This effect is clearly evident in Fig. 4 where this data is shown by the solid symbols. From the data at the lower temperatures, an activation energy of approximately 125 kJ $mole^{-1}$ was calculated and is in agreement with that observed at the higher sulfur potential.

At the lowest sulfur potential studied (1.5×10^{-4} Nm^{-2}), the reaction rates are the lowest and decrease with increasing temperature, as seen in Fig. 3. The change in slope in the two lower curves of Fig. 3 are the result of changes deliberately made in the sulfur potential. At the breaks, the

sulfur potentials were increased from 1.5×10^{-4} Nm^{-2} to 10^{-3} Nm^{-2} by changing the ratio of H_2 to H_2S. This was done in order to test whether an increase in sulfur potential had the expected effect on the sulfidation rate — an increased rate of reaction with an increase in the sulfur potential at a constant temperature — which it does. The functional dependence of the parabolic rate constant on temperature is plotted in Fig. 4 by the square symbols. It is seen that the rate of reaction decreases abruptly from 1065 K to 1145 K with a further slight decrease at 1230 K.

Layered Sulfide Scales

At all temperatures and sulfur potentials investigated, the sulfide scales consisted of either one or two outer layers in addition to a subscale or a zone of internal sulfidation. This is shown in Fig. 5 for scales formed in a sulfur potential of 1.4×10^{-2} Nm^{-2} at 1145 K and at 1226 K. The outer layer nearest to the subscale will be termed outer layer I (OL-I) while the outermost layer of the layered scale will be referred to as outer layer II (OL-II).

A correlation between the number of outer layers formed in the scale and the kinetic behavior of sulfidation was observed. The two outer layers were present only when the normal increase in the rate of sulfidation with temperature was found (Fig. 4). When only one outer layer was present, the rate of reaction was found to decrease with increasing temperature or the reaction rate was independent of temperature (Fig. 4). Thus, the sudden decrease in the reaction rate with increasing temperature appears to be associated with the transition in the layered sulfide scales from two outer layers to one outer layer.

In general, all sulfide scales appeared to be porous with interface regions between different scale layers being more porous. In most cases, the interface regions contained large fissures and often separated from each other as a result of mechanical and/or thermal stresses. The relative thickmess of the scale layers including the subscale were found to depend on both temperature and sulfur potential.

Sulfide Phases

The various layers of the sulfide scale were mechanically separated and examined using X-ray diffraction analysis. The subscale was adherent to the unreacted alloy and had to be removed by scraping. The sulfide phases were identified by comparing diffraction patterns with the ASTM powder data file or other relevant compilations available in the literature.[3] Because of the complex nature of the scaling layers, it was only possible to identify the major phases present by this technique. More accurate and detailed analysis was possible by the critical examination of the microstructure of the scales and by compositional analysis of different phases using both energy dispersive X-ray and microprobe analyses.

In all the scales where two outer layers were obtained, the outermost layer (OL-II) contained phases that were primarily of the Fe-Ni-S system. Two common phases were a phase containing monosulfide solid solution $(Fe, Ni)_{1-x}S$, apparently formed out of pyrrhotite ($Fe_{1-x}S$) and Millerite ($Ni_{1-x}S$), and a phase known as Pentlandite $(Fe, Ni)_{9-x}S_8$. The OL-II layer formed below 1065 K contained both of these phases. At higher temperatures, however, only Pentlandite was identified and this phase melted around 1145 K. The melt upon solidification separated into two phases, a metallic phase containing nearly

equal amounts of iron and nickel and a sulfide phase with the Pentlandite composition, $Fe_{4.5}Ni_{4.5}S_8$.

The X-ray analysis of the first outer layer (OL-I) indicated the presence of an iron chromium sulfide spinel ($FeCr_2S_4$, Daubreelite). The actual composition of this phase, as determined by the electron microprobe analysis, was different from the exact spinel composition.[1] A careful microstructural examination of this layer, however, revealed arrays of alternate sublayers in the slowly cooled samples. The sublayers were absent with quenched samples. These sublayers could not be separated mechanically and thus, the X-ray analysis could not be made on the individual sublayers. By microprobe analysis it was deduced that the sublayers differed only in the Fe:Cr ratio and that all phases belong primarily to Fe-Cr-S system.

Subscale formation was found to be due to internal sulfidation and hence, is an agglomerate of sulfide phases in a metal matrix. The sulfide phases are primarily the spinel and the chromium sulfides with the latter present mainly at the interface of the unreacted metal and the subscale. Additionally, the formation of manganese sulfide and the enrichment of silicon was indicated in the subscale. The chromium sulfur system is very complex and has a number of phases; each stable in a narrow range of composition.[4] For this reason it was not possible to ascertain the exact phases present in the subsurface scale by X-ray diffraction analysis alone. From a combination of energy dispersive X-ray analysis and microprobe analysis, it was determined that the chromium sulfide phase present is either Cr_2S_3 or Cr_5S_6. Additionally, small amounts of iron dissolved in the phase made the analysis even more difficult and ambiguous. Finally, the depth of the internal sulfidation zone, the composition of the

sulfide phases, and the composition of metal surrounding the sulfide are dependent on the temperature as well as the partial pressure of sulfur.

Microstructure and Composition of Scales

The microstructure of the sulfide scales was observed by examining the metallographically polished cross sections of the samples. In most cases the scales flaked off during cooling. Such samples were collected and examined separately from the unreacted alloy. The cross sections were examined employing optical as well as scanning electron microscopy. The microstructural variations within the scale with respect to the layered structure and variations within the individual layers with respect to temperature and pressure were studied. The compositional changes associated with the microstructural variations were determined by either energy dispersive X-ray analysis or by electron microprobe analysis.

Variations in the Outermost Layer (OL-II)

The microstructure of OL-II formed at 933 K in a sulfur potential of 1.4 x 10^{-2} Nm^{-2} is shown in Fig. 6. Samples reacted below 1000 K at all sulfur potentials exhibited similar microstructures. Two distinctly different phases were observed. The brighter phase seen in Fig. 6a is the exsolved Pentlandite phase in the form of lamellae along the darker phase of Pyrrhotite and Millerite in solid solution. This microstructure is similar to that reported earlier by Craig[5] and Kullerud.[6] The composition of the exsolved Pentlandite phase is shown in Fig. 6b whereas the composition of the solid solution phase is shown in Fig. 6c. The nickel content of the latter was observed to vary from 10 to 14 wt. % depending on the temperature and pressure of sulfidation.

Samples reacted at 1065 K in a sulfur potential greater than 1.4×10^{-2} Nm^{-2} did not show the two phase separation and the X-ray analysis showed the formation of Pentlandite, $(Fe, Ni)_9S_8$. Compositional analysis indicated, however, that the iron and nickel contents are not equal. The exact composition of this phase, at this temperature, was found to be represented as $Fe_{5.8}Ni_{3.2}S_8$. The difference between the monosulfide solid solution and the Pentlandite phase is the sulfur content, which is 41 and 38 wt. %, respectively. Upon further increasing the temperature, Pentlandite constituting the outermost layer melted and the melt collected as globules adhering to the bottom portion of the hanging sample. The cross section of one such globule formed at 1230 K in a sulfur potential of 39 Nm^{-2} is shown in Fig. 7. Similar observations were recorded for all the samples reacted above 1145 K with sulfur potentials greater than 2×10^{-2} Nm^{-2}. Upon solidification the melt separated into two phases; a metallic phase constituting primarily of nickel and iron and a sulfide phase with the composition $Fe_{4.5}Ni_{4.5}S_8$ (Pentlandite) as shown in Fig. 8. The bright regions in Fig. 8a represent the metallic phase and the grey regions represent the sulfide phase. The absence of sulfur in the bright phase is indicated in Fig. 8b where Kα X-ray intensity image for sulfur is mapped. The compositions of these two phases are compared in Fig. 8c where the dotted pattern represents the bright phase and the bars represent the grey phase. The average composition of the overall melt was calculated by measuring relative areas of these two phases in a number of representative micrographs. The composition was found to be 27 wt. % S, 35 wt. % Fe, 38 wt. % Ni. This composition is very close to that reported by Kullerud.[6] The maximum chromium content of any phase in OL-II was not more than 4 wt. %.

Pentlandite, when melted at higher temperatures, penetrated the grain boundaries of OL-I. Upon cooling the grain boundaries of OL-I were found to be cemented by the melt and the localized transgranular cracks had developed due to thermal and mechanical stresses as shown in Fig. 9.

Variations in the Outer Layer (OL-I)

The highly peculiar nature of OL-I is shown in Fig. 10a and is the result of the presence of alternate arrays of sublayers. These sublayers are lamellar in nature and look like a network of twin structures meeting at the grain boundaries. Exsolved nickel and iron, segregated at the grain boundaries, served as a vertex for the angularly arrayed sublayers. Each sublayer is in the form of a band, with bandwidth becoming wider as the band approaches the subscale. The sublayers were either less pronounced or absent when the samples were quenched from the test temperature, as shown in Figs. 10b and 10c. These micrographs (Figs. 10b and 10c) were taken from the same sample, with the former observed nearer to OL-II and the latter observed nearer to the subscale. All the photomicrographs of Fig. 10 belong to the samples reacted at identical conditions ($T = 1145$ K, $P_{S_2} = 1.4 \times 10^{-2}$ Nm^{-2}), but with differing cooling rate. The sublayers were absent in samples reacted below 1000 K. The microstructure and the composition of OL-I, formed at 933 K in a sulfur potential of 1.4×10^{-2} Nm^{-2} and slowly cooled, is shown in Figs. 11a and 11b, respectively.

The compositions of the two sublayers shown in Fig. 10a are compared in Fig. 10a'. The compositions of the light grey and the dark grey regions are represented by dots and bars, respectively. As can be seen, the sulfur content and the Fe:Cr ratio differed in two phases. The average composition of these sublayers is identical and is equal to that of the overall composition

of the quenched samples, Fig. 10b', thus indicating that these sublayers are formed only during cooling. In samples formed at lower temperatures (910 and 930°C), OL-I contains, primarily, the chromium sulfide phase, Cr_2S_3, with very little iron present, as is seen in Fig. 11b. These results suggest that different phases constitute OL-I at different temperatures.

Another interesting feature of OL-I is the segregation of nickel and iron at the grain boundaries (Fig. 10a), or as separate patches within the layer but close to the grain boundaries as shown in Fig. 12. In the quenched samples (Fig. 10a) the grain boundary width is smaller than that of the slowly cooled samples (Fig. 10b). Additionally, whenever nickel and iron were segregated as separate patches, the grain boundary width was smaller, as is shown in Fig. 12.

Variations in the Subscale

The subscale is composed mainly of the sulfide inclusions in a metal matrix. The metal phase is rich in iron and nickel, whereas the sulfide phase is rich in chromium. The depth of the subscale, as well as the distribution and composition of the two phases were found to depend on the sulfur potential and temperature. At lower temperatures and higher sulfur potentials the sulfide phase in the subscale was abundant and the penetration depth was shorter. At higher temperatures and lower sulfur potentials the subscale contained finely dispersed sulfide particles and the depth of the subscale was larger. A careful analysis indicated that the nature of the subscale is dependent mainly on the composition of OL-I. An increase in the chromium content of OL-I, increased the penetration depth. A more detailed analysis of the subscale is being reported elsewhere.[7]

COMPOSITION PROFILES

Concentration profiles across the sulfide scales were established by using either electron microprobe analysis or energy dispersive X-ray analysis. In both cases, point analysis was performed and the compositions represented the average compositions, i.e., the sublayers of OL-I were not separated for analysis. The composition profiles of the scales formed in a sulfur potential of 1.4×10^{-2} Nm^{-2} and at 933 K, 1145 K and 1285 K are shown in Figs. 13a, b, and c, respectively. The temperature 1145 K is the transition temperature (Fig. 4) and above this temperature only one outer layer is formed and is accompanied by a decrease in reaction rate. Although the analysis was performed for all the elements present in 310 stainless steel, profiles of the major elements (Fe, Ni, Cr and S) are shown in Fig. 13. It is seen that the nickel content of OL-II increases with temperature until OL-II disappears. The Fe:Cr ratio of OL-I generally decreases with temperature. The scale formed at 933 K and $P_{S_2} = 1.4 \times 10^{-2}$ Nm^{-2} is an exception in that it contained essentially pure chromium sulfide, Cr_2S_3. (The same was observed for scales formed at 910 K in a sulfur potential of 39 Nm^{-2}.)

DISCUSSION

Outer Layer II (Fe-Ni-S)

The Outer Layer II formed in the sulfidation of 310 stainless steel consists primarily of Fe-Ni-S. Assuming that small amounts of chromium (<2 wt. %) observed in this layer will not drastically change the phase relations of this system, the observations of the present study can be compared with the phase relations of the ternary Fe-Ni-S system. This system interested the geologists

for its mineralogical significance. Consequently, a voluminous amount of literature is available; however, only those studies which have some direct bearing on the present results will be considered here.

The ternary Fe-Ni-S system is complicated by the presence of several phases and solid solutions. The phase relations for this system in the temperature range from 375 K to 1375 K have been reported by Kullerud.[6,8] Two of these phases--a solid solution of the monosulfides of iron and nickel and Pentlandite--were observed in the present study. Other phases such as Valerite (Ni_2FeS_4), Bravoite ($(Fe,Ni)S_2$), Pyrite (FeS_2), Vaesite (NiS_2), Smythite (Fe_3S_4) and Polydymite (Ni_3S_4) were not observed. Some of these phases exist only at lower temperatures and the others form only under higher sulfur potentials than those used in the present study.

The monosulfide solid solution extends across the system from $Fe_{1-x}S$ to $Ni_{1-x}S$ without a miscibility gap.[9] This phase can coexist with Pentlandite even to temperatures as low as 475 K.[3] During the present investigations, such a mixture was observed (Fig. 6b). The exsolution of Pentlandite in the form of lamellae and veinlets can result from cooling the initially homogeneous monosulfide solid solution.[5] The exsolution is very rapid and can be observed even in the quenched samples.[3] The general composition of this phase was found to be 46 wt. % Fe, 14 wt. % Ni and 40 wt. % S and is in excellent agreement with the values reported by Shewman and Clark.[3] Shewman and Clark[3] also reported the formation of two monosulfide solid solutions at lower temperatures (<475 K) with compositions 47, 14, 39 wt. %; and 18, 45 and 37 wt. % Fe, Ni and S, respectively. They conclude, however, that at higher temperatures these two phases approach the composition of each other. In the present study we observed only one monosulfide solid solution.

Kullerud[6] reported the existence of a homogeneous liquid phase of composition pertinent to the formation of Pentlandite - Pyrrhotite or Pentlandite-Hazelwoodite (Ni_3S_2) up to a temperature of 1375 K. Upon cooling, the monosulfide solution crystallizes first from the liquid and co-exists down to 1135 K with a metal rich iron-nickel-sulfur liquid. Below 883 K the Pentlandite-Pyrrhotite pairs become stable. Between 883 K and 1135 K the Pentlandite of composition $Fe_{4.5}Ni_{4.5}S_8$ decomposes to $(Fe,Ni)_{1-x}S$ having the hexagonal Pyrrhotite structure and to a high temperature, non-quenchable phase equivalent to $Ni_{3-x}S_2$ but containing some iron. In the present study the sample reacted at 1065 K in a sulfur potential of 1.4×10^{-2} Nm^{-2} has the actual composition $Fe_{5.8}Ni_{3.2}S_8$ indicating that this phase might be composed of a mixture of $Fe_{1-x}S$ and Ni_3S_2; however, upon cooling this composition might have transformed to Pentlandite. Kullerud[6] also observed the melting of synthetic Pentlandite at 1135 K yielding a metal rich, iron-nickel-sulfur liquid ($\simeq$ 20% S).

More recently, Conrad et al.[10] reported their investigations on the stability of Pentlandite using differential thermal analysis. According to their observations Pentlandite undergoes the following transformation:

$$\text{Pentlandite} \xrightarrow{890K} \text{mss} + \text{HS} \xrightarrow{1130K} \text{mss} + \text{L}.$$

It was also found that these transformations are reversible and one would expect that Pentlandite reforms after cooling. In our experiments the formation of liquid was observed which upon solidification gave two phases (Fig. 8)--a sulfide phase (Pentlandite) and a metal phase (iron and nickel) as shown in Fig. 8.

While the observations of the present study are in general agreement with the existing literature, two discrepancies were observed. First, the Pentlandite

phase was observed above 833 K. For example, the exsolved Pentlandite occurred with the monosulfide solid solution in the scale formed at 933 K (Fig. 6b). This may be explained in terms of sulfur potentials where, at lower sulfur potentials, the formation of Pentlandite is favored, as has been observed by Naldrett, Craig and Kullerud.[8] Secondly, it is difficult to understand why Pentlandite--observed to decompose above 833 K — was found to melt at 1145 K. One potential explanation may be that Pentlandite is stable only under certain metal and sulfur activities and, thus, may be considered a compound formed of Pyrrhotite and Hazelwoodite. At higher temperatures and lower sulfur potentials the Pyrrhotite and Hazelwoodite decompose giving iron and nickel, increasing the metal activity and stabilizing the Pentlandite phase. Thermodynamically, Hazelwoodite could decompose, thus resulting in a high nickel content in the melt of Pentlandite. This explanation is consistent with the observations of Shewman and Clark[3] in that Pentlandite is marked by the presence of (Ni,Fe) in the solid solution. It is also to be pointed out that in the present study the reaction was carried out under dynamic conditions in contrast to the other investigators where the experiments were carried out in sealed tubes. However, the basic agreement of the results with the existing literature lends confidence that the gas phase equilibrium in the present experimental conditions is adequate, while the metal activities are controlled by the diffusion rates.

Outer Layer I (Fe-Cr-S)

The outer layer I consists primarily of Fe-Cr-S. Additionally, small amounts of nickel present in this layer at low temperatures and high sulfur potentials seem to play some role. Unlike the Fe-Ni-S system, very little information is available on this ternary system. Vogel and Heuman[11] suggested

that Daubreelite is formed out of Triolite (FeS) and CrS according to the reaction

$$2FeS + 2\ CrS = FeCr_2S_4 + Fe \qquad (3)$$

However, Ramdohr[12] maintains that the formation of free iron from this reaction is very unlikely and alternatively suggests that FeS-$FeCr_2S_4$ forms a binary join with complete solid solution. The position of the solvus has yet to be determined as the FeS phase is triolite rather than Pyrrhotite. Although complete mixing of Triolite and Daubreelite was assumed at high temperatures, unmixing of the solid solution was found during cooling by Ramdohr.[12] In some meteorites, Daubreelite and Triolite were found as essentially pure phases in neighboring grains without any sign of a mixed crystal formation. In most cases, however, Ramdohr[12] observed exsolution textures in polished sections.

During the present investigation we have observed a number of different phases at different temperatures. Samples reacted around 900 K formed a chromium sulfide phase with the composition Cr_2S_3. Very little amounts of iron were present in this phase, suggesting that neither a solid solution of FeS-CrS or FeS-Cr_2S_3 nor a compound of $FeCr_2S_4$ formed at these temperatures. Above 1000 K the OL-I contained Fe-Cr-S sublayers (Fig. 10), which differed only in the Fe:Cr ratio. From the quenching experiments it was deduced that these sublayers were exsolved structures formed during cooling. However, the sublayers do not have compositions near Daubreelite. We, therefore, suggest that, at the reaction temperature, OL-I is made up of a solid solution of FeS-NiS-CrS. Upon cooling, the following reaction occurs;

$$4(CrS\ FeS\ NiS) = 2\ (Cr,\ Fe)S + FeCr_2S_4 + FeNi \qquad (4)$$

Because of the high diffusion rates in these sulfides, the nickel and iron migrate to the energetically favorable locations such as the grain boundaries. An increase in temperature then increases the chromium content of the $(Fe,Cr)_{1-x}S$ phase. Finally, at temperatures above 1145 K and at sulfur potentials less than the sulfur potential above FeS, the formation of sulfides rich in chromium is observed.

From our experimental observations it is tentatively suggested that the pseudobinary joins of FeS and CrS do not show any continuous solid solution around 900 K. Above 1145 K, under favorable sulfur potentials, the chromium content of $(Fe,Cr)_{1-x}S$ increases and the rate of sulfidation was decreased in relation to the chromium content. A more detailed thermodynamic analysis for all the phases in the system is being carried out.

Subscale

As was pointed out in an earlier publication,[1] subscale growth is facilitated by a dissociation mechanism similar to that originally proposed by Dravnieks and McDonald[13] and by Meussner and Birchenall.[14] The partial pressure of sulfur at the interface of the unreacted alloy and OL-I is dependent on the composition of OL-I and temperature. From the present experimental observations it is clear that the composition of OL-I is dependent on both temperature and the external sulfur potential at which the reaction is carried out. Therefore, the subscale is also dependent on the sulfur potential and temperature and a more detailed analysis of the subscale will be given elsewhere.[7]

Influence of Scaling Layers on Reaction Kinetics: Role of Chromium

In a previous study[1] it was shown from the marker experiments that the sulfidation of 310 stainless steel is controlled by the diffusion of metal ions through the sulfide scale. Since the scales are multilayered, diffusion through one of these layers will be the rate controlling step. During the course of this investigation, OL-II changed from solid to liquid at the transition temperature, under favorable sulfur potentials, and finally disappeared. Fig. 14 shows the melt formed at a temperature of 1145 K in a sulfur potential of 1.4×10^{-2} Nm^{-2}. The melt has collected at the bottom portion of the hanging sample. Consequently, OL-II is thick at the lower end of the sample (Fig. 14c) and is absent at the upper end (Fig. 14a). If the diffusion through OL-II were the rate controlling step, it is expected that the thickness of OL-I would change with respect to the sample position. On the contrary, OL-I is seen in Fig. 14 to have a uniform thickness throughout the length of the sample. Additionally, the composition of OL-I was found to be the same at all positions of the sample at a given depth, indicating that the diffusion through OL-II is not the rate controlling step. The decrease of the reaction rate with the disappearance of OL-II (Fig. 4) is thought to be purely a circumstantial coincidence.

The decrease in the reaction rate with increasing temperature can also result if there are some species vaporizing and the vapor pressure becomes considerable when the temperature is increased. However, thermodynamic analysis did not reveal the presence of any such species. Moreover, duplicate experiments were performed with a collector plate at the cold end of the exit gases. No material other than sulfur was observed to condense on the collector plate.

A careful analysis of the results has shown that the sudden decrease of the reaction rate (Fig. 4) is also associated with the decrease in the Fe:Cr ratio as shown in Fig. 15. In this figure the Fe:Cr ratio of OL-I is shown, as a function of the reciprocal of the absolute temperature, for the three sulfur potentials investigated. It is seen from Fig. 15 that a sudden change in Fe:Cr ratio occurs at the two lower sulfur potentials, indicating the formation of a new phase which is more protective than the prior phase. It is, therefore, interesting to plot the reaction rate as a function of Fe:Cr ratio for these two sulfur potentials and this is shown in Fig. 16. The data are reasonably linear at each potential, indicating that diffusion through OL-I is the rate controlling step for which Fe:Cr ratio is critical. Once this critical composition has been reached, the reaction rate is independent of temperature. On the basis of these observations, the decrease in the reaction rate with increasing temperature can be explained. Increase in temperature increases the dissociation pressure of $(Fe,Cr)_{1-x}S$, resulting in the formation of a more chromium rich phase. The reaction rate is controlled by the Fe:Cr ratio which is dependent on both the temperature and the external sulfur potential. This is in complete agreement with the results obtained at a sulfur potential of 39 Nm^{-2}, which did not show any abnormalities either in the reaction kinetics or Fe:Cr ratio. The nature of the subscale formation is also closely associated with the changes in OL-I.[7]

CONCLUSIONS

At a given temperature and sulfur potential the weight gain obeyed the parabolic rate law after an initial transition period.

When the log of the parabolic rate constant is plotted, as a function of the reciprocal of the absolute temperature, a break in the curves was observed around 1145 K for $P_{S_2} \leq 10^{-2}$ Nm^{-2}. This temperature, at which the break occurred, was termed a transition temperature.

Below the transition temperature, the activation energy was found to be approximately 125 KJ $mole^{-1}$. Above the transition temperature the rate of sulfidation was independent of temperature but dependent on the Fe:Cr ratio in the iron-chromium-sulfide layer of OL-I.

Below the transition temperature the diffusion of Fe and Ni through OL-I contribute to the scale formation, whereas above the transition temperature the diffusion of chromium through OL-I controls the scale formation.

ACKNOWLEDGEMENTS

The authors wish to thank Mr. Dell P. Williams, Dr. K. T. Jacob and Prof. Austin Chang for their suggestions. The authors are thankful to Dr. Kenneth Snetzinger and Mr. Richard Lindberg for the analysis of samples using electron microprobe and energy dispersive X-rays. Invaluable assistance of Mr. John Mossberg, Mr. Larry Pezzolo and Mr. James Stein is gratefully acknowledged. Mr. A. V. Levy is thanked for his keen interest in this work. This research is sponsored by the Division of Physical Research, ERDA and the Materials and Physical Sciences Branch, NASA-Ames Research Center.

REFERENCES

1. D. Bhogeswara Rao and Howard G. Nelson, "Sulfidation of 310 Stainless Steel at Sulfur Potentials Encountered in Coal Conversion Systems," NASA Technical Memorandum NASA TM X-73,166, September 1976, and the Proceedings of the symposium on "Properties of High Temperature Alloys," Eds. Z. A. Foroulis and F. S. Pettit, proceedings Vol. 77-1, The Electrochemical Soc., Inc., Princeton, N. J. (1971) pp. 464-493.
2. "JANAF" Thermochemical Tables, NSRDS-NBS 37 (1974).
3. R. W. Shewman and L. A. Clark, *Can. J. Earth Sciences*, 7, 67 (1970).
4. F. Jellinek, *Acta Cryst.*, 10, 620 (1957).
5. J. R. Craig, *Amer. J. Sci.*, 273-A, 496 (1973).
6. G. Kullerud, *The Can. Mineralogist*, 7, 353 (1963).
7. D. Bhogeswara Rao, K. T. Jacob, H. G. Nelson and R. Lindberg, in preparation.
8. L. A. Clark and G. Kullerud, *Econ. Geol.*, 58, 853 (1963).
9. A. J. Naldrett, J. R. Craig and G. Kullerud, *Econ. Geol.*, 62, 826 (1967).
10. B. R. Conrad, R. Sridhar and J. S. Warner, High Temperature Enthalpies of Some Nickel Sulfides, 106th AIME Annual Meeting, Atlanta, Georgia, March 7-11, 1977.
11. R. Vogel and Th. Heumann, Übes Daubreelith. *Neus Jahb. Mineral., Montash*, 175-190 (1950).
12. P. Ramdohr, "Opaque Minerals in Stony Meteorites," Carnegie Institute, Washington Year Book, 217, 1963.
13. A. Dravnieks and H. McDonald, *J. Electrochem. Soc.*, 94, 139 (1948).
14. R. Meussner and C. Birchenall, *Corrosion Sci.*, 13, 677 (1957).

FIGURE CAPTIONS

Fig. 1. Parabolic plots for the sulfidation of 310 stainless steel at a sulfur potential of 39 Nm^{-2}. Filled circles indicate the formation of liquid in the OL-II.

Fig. 2. Parabolic plots for the sulfidation of 310 stainless steel at a sulfur potential of 1.4×10^{-2} Nm^{-2}. Filled circles indicate the formation of liquid in the OL-II.

Fig. 3. Parabolic plots for the sulfidation of 310 stainless steel at a sulfur potential of 1.5×10^{-4} Nm^{-2} and higher.

Fig. 4. Influence of temperature on the parabolic rate constant for the sulfidation of 310 stainless steel.

Fig. 5. Multilayered sulfide scales formed during the sulfidation of 310 stainless steel. (a) Scale formed at 1145 K and in a sulfur potential of 1.4×10^{-2} Nm^{-2}. (b) Scale formed at 1226 K and a sulfur potential of 1.4×10^{-2} Nm^{-2}.

Fig. 6. Microstructure and the composition of OL-II formed at a sulfur potential of 1.4×10^{-2} Nm^{-2} and 933 K. (a) Composition of the grey phase (46 wt. % Fe, 13 wt. % Ni and 41 wt. % S). (b) Microstructure showing the exsolved lamellae of Pentlandite (bright phase). (c) Composition of the bright phase (30 wt. % Fe, 29 wt. % Ni and 38 wt. % S).

Fig. 7. Cross section of the metal-rich, iron-nickel-sulfur melt formed at 1230 K and a sulfur potential of 39 Nm^{-2}.

A-3058

Fig. 8. Separation of two phases upon solidification of a melt formed in a sulfur potential of 1.4×10^{-2} Nm^{-2} at 1145 K. (a) Microstructure of the solidified melt. (Bright and grey phases are the metal and the sulfide phases, respectively.) (b) X-ray intensity image for the K_{α} radiation of sulfur showing the absence of sulfur in the bright phase. (c) Comparison of the compositions of metal and sulfide phases. Dotted pattern represents the bright phase and bars represent the grey phase.

Fig. 9. Penetration of melt through the grain boundaries of OL-I at 1230 K and a sulfur potential of 39 Nm^{-2}.

Fig. 10. Effect of cooling rate on the formation of sublayers in OL-1. T = 1145 K, $P_{S_2} = 1.4 \times 10^{-2}$ Nm^{-2}. (a) Slowly cooled sample showing the sublayers. (b) and (c) Disappearance of sublayers in the quenched samples. (a') Compositions for the individual sublayers of Fig. 10a. Light grey phase = 14 wt. % Cr, 41 wt. % Fe, 43 wt. % S and 1 wt. % Ni. Grey phase = 26 wt. % Cr, 27 wt. % Fe, 46 wt. % S and 0.5 wt. % Ni.
(b') General composition of OL-I shown in Fig. 10b (19.5 wt. % Cr, 33.5 wt. % Fe, 2 wt. % Ni, 44 wt. % S).

Fig. 11. Absence of sublayers for certain compositions of OL-I. (a) Microstructure of OL-I formed at 933 K and a sulfur potential of 1.4×10^{-2} Nm^{-2}. (b) Composition of OL-I shown in Fig. 11a.

Fig. 12. Segregation of metal phase along and near the grain boundaries. (a) Microstructure and composition of the exsolved metal phase (36 wt. % Fe, 62 wt. % Ni, 1 2t. % Cr).

A.7056

Fig. 13. Distribution profiles for iron, nickel, chromium and sulfur in the sulfide scales formed at a sulfur potential of 1.4×10^{-2} Nm^{-2}. (a) 933 K, (b) 1145 K and (c) 1280 K.

Fig. 14. Micrographs showing the melting of OL-II and its influence on the other layers of the scale. ($T = 1145$ K, $P_{S_2} = 1.4 \times 10^{-2}$ Nm^{-2}).

Fig. 15. Fe : Cr ratio of OL-I plotted as a function of the inverse of the absolute temperature.

Fig. 16. The dependence of parabolic rate constants on the Fe : Cr ratio of OL-I.

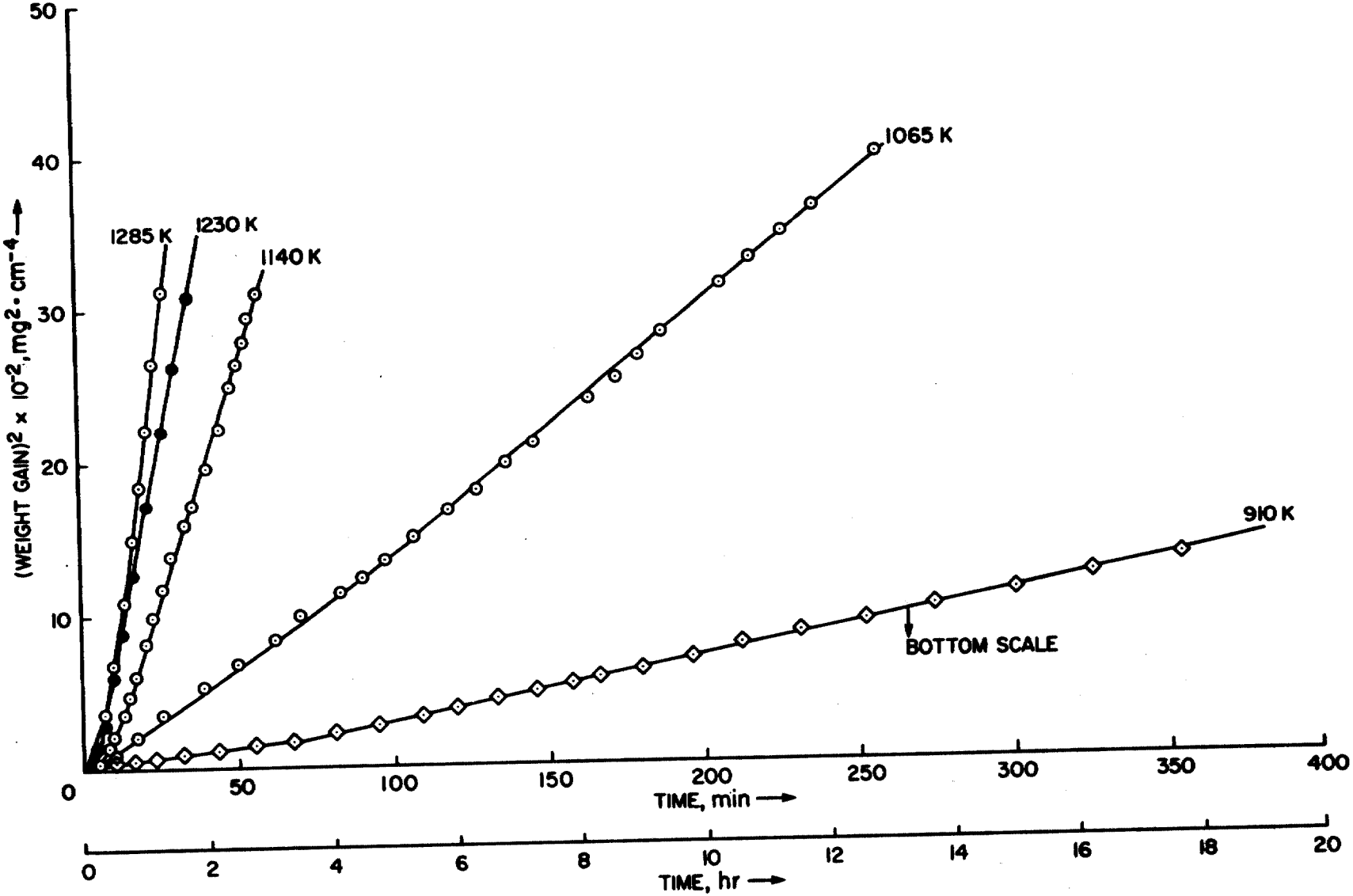

Fig. 1. Parabolic plots for the sulfidation of 310 stainless steel at a sulfur potential of 39 Nm^{-2}. Filled circles indicate the formation of liquid in the OL-II.

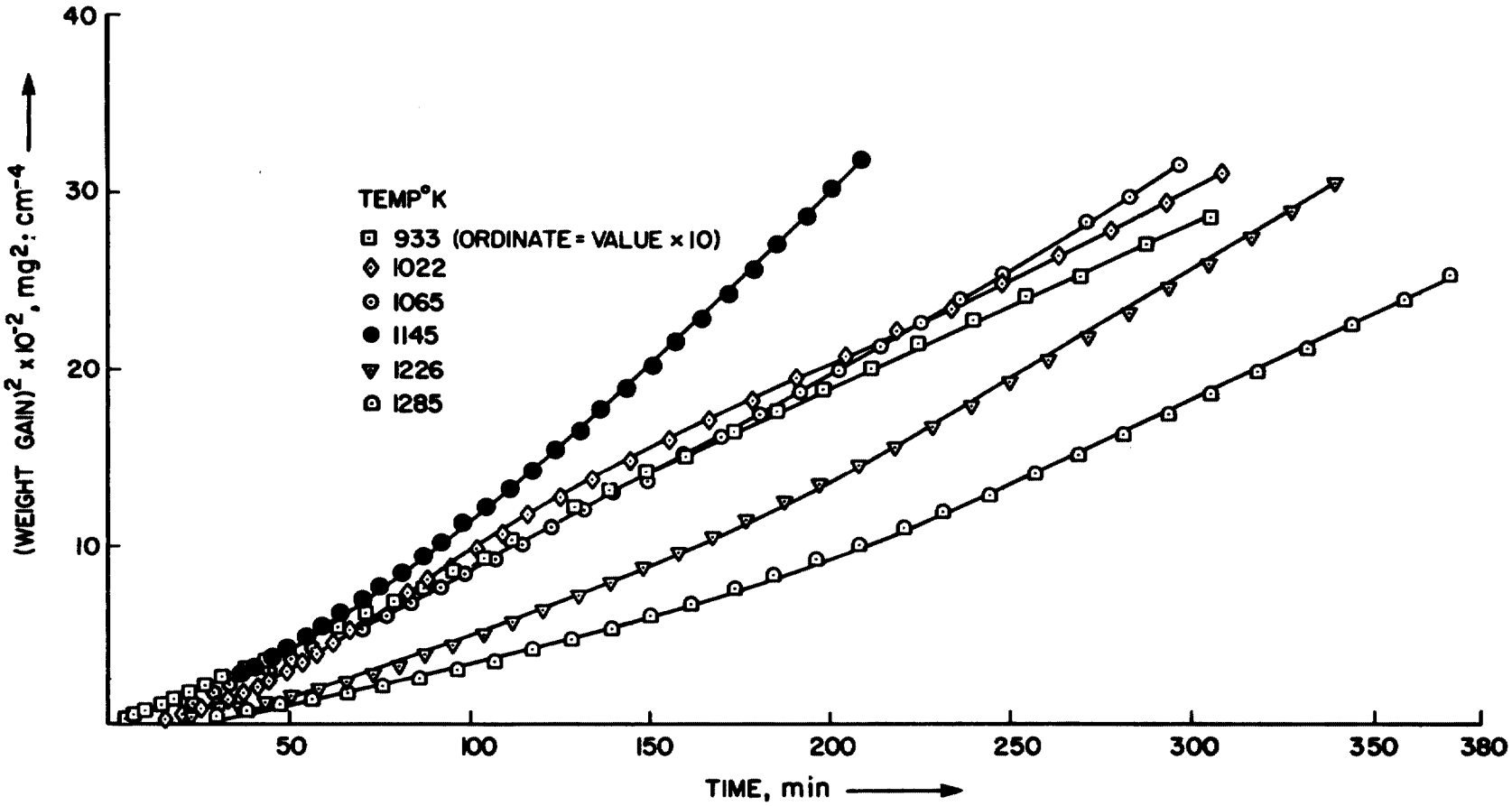

Fig. 2. Parabolic plots for the sulfidation of 310 stainless steel at a sulfur potential of 1.4×10^{-2} Nm^{-2}. Filled circles indicate the formation of liquid in the OL-II.

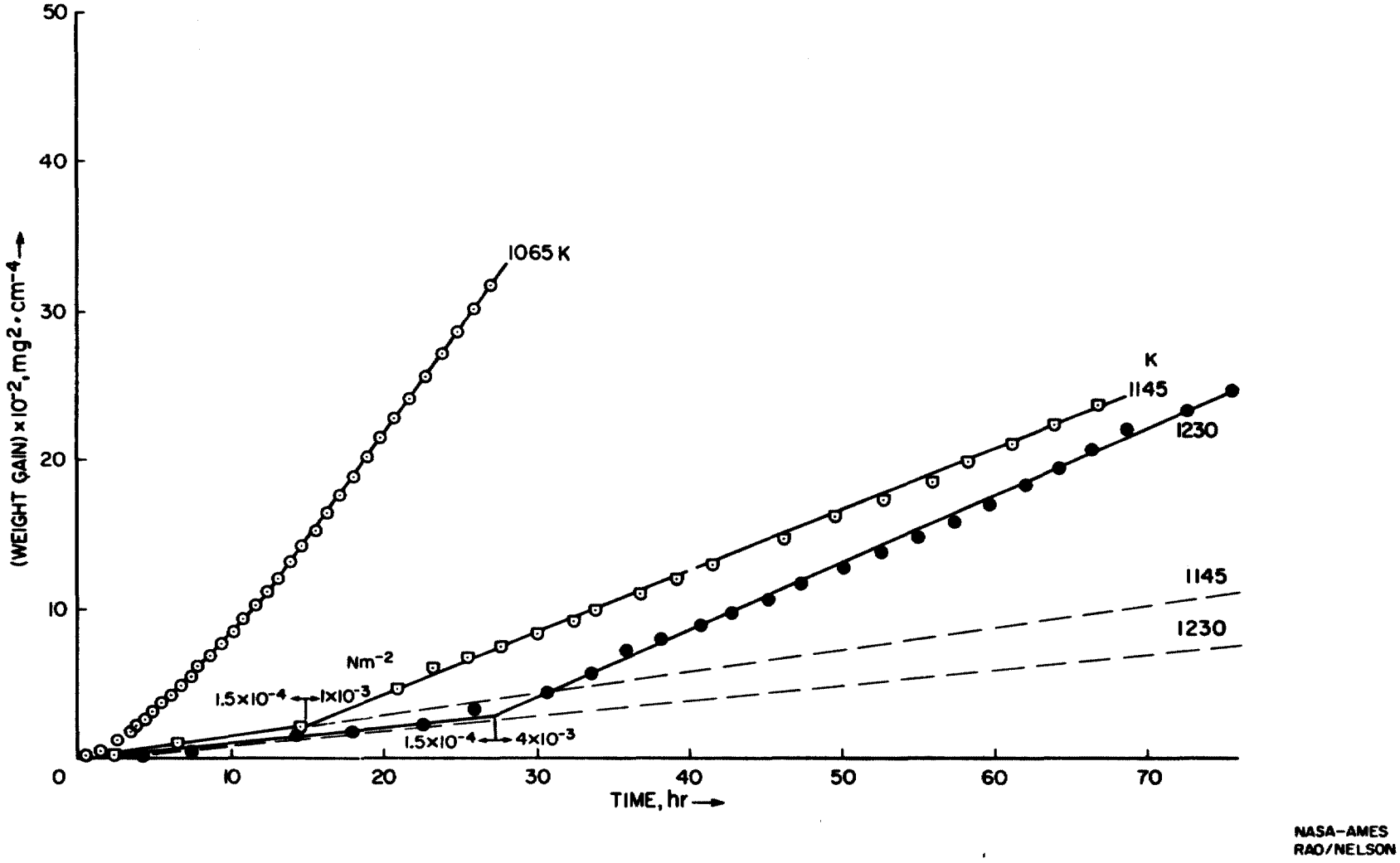

Fig. 3. Parabolic plots for the sulfidation of 310 stainless steel at a sulfur potential of 1.5×10^{-4} Nm^{-2} and higher.

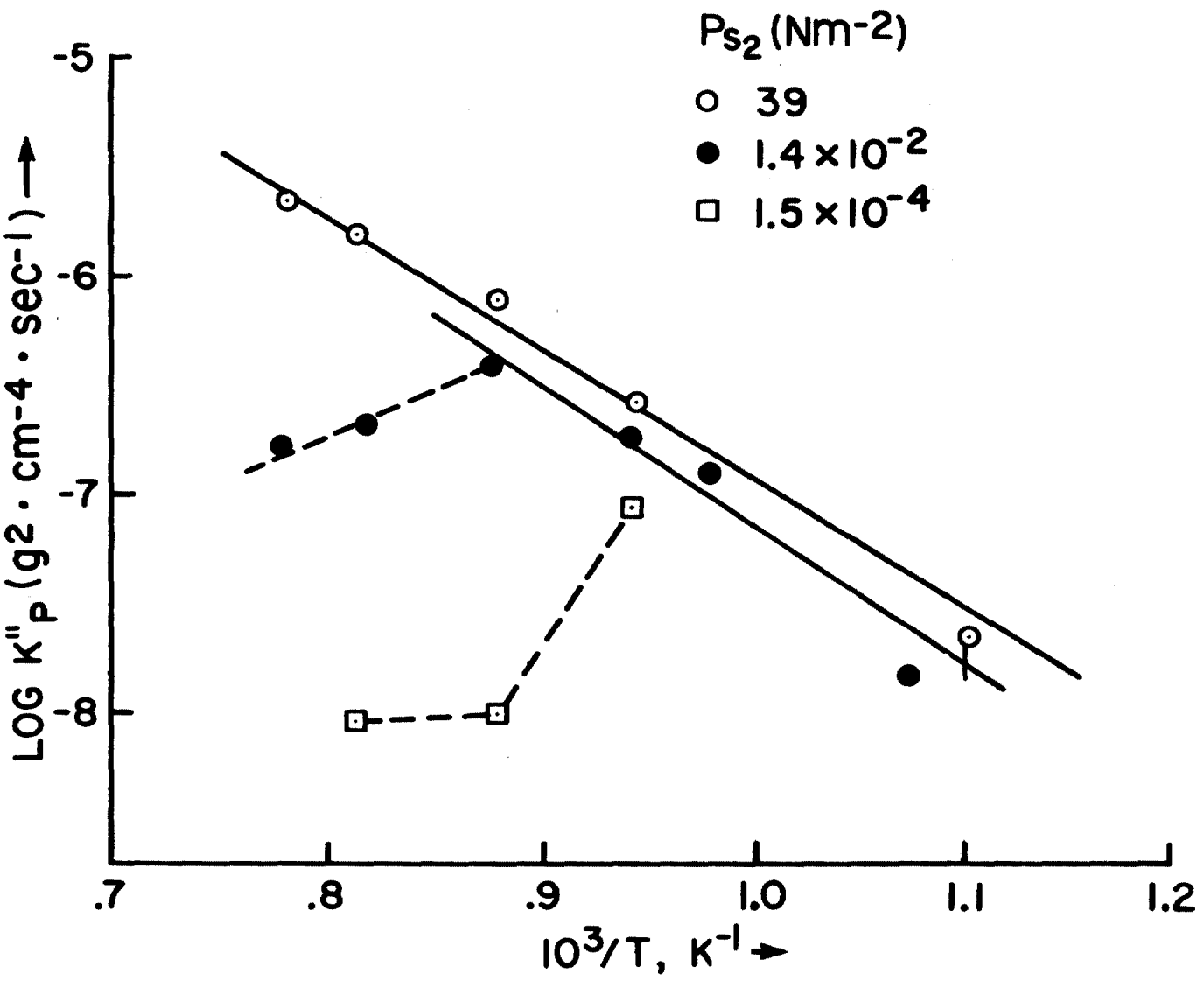

Fig. 4. Influence of temperature on the parabolic rate constant for the sulfidation of 310 stainless steel.

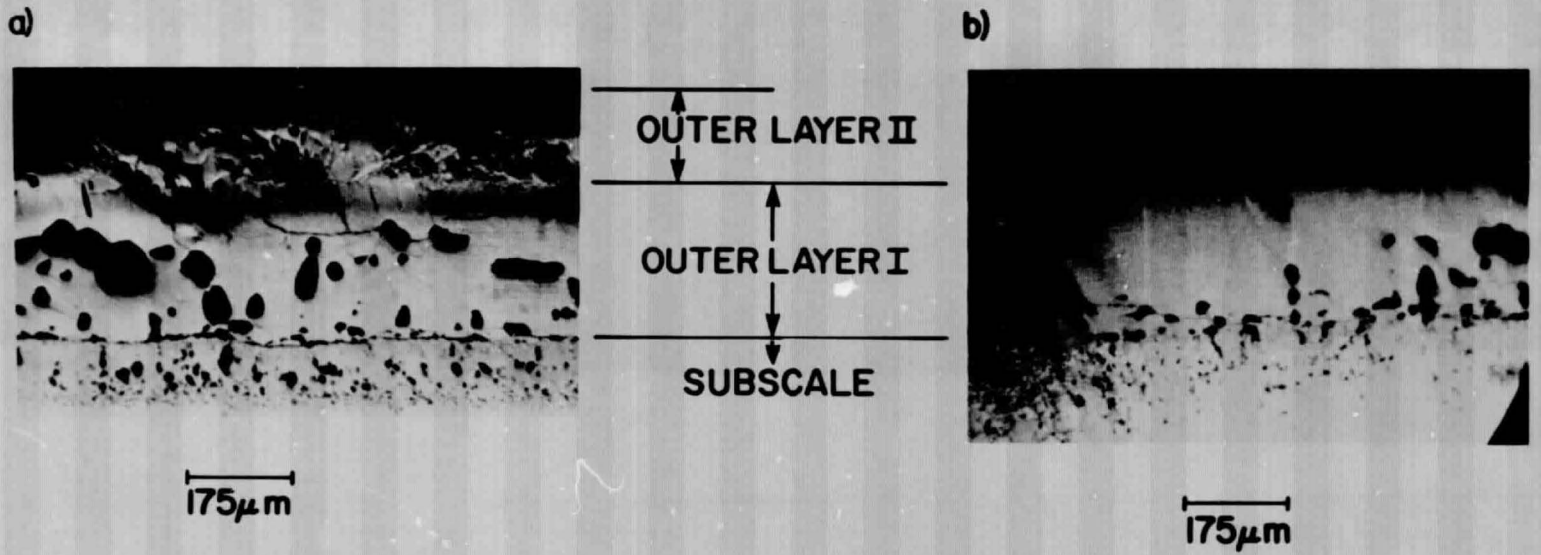

Fig. 5

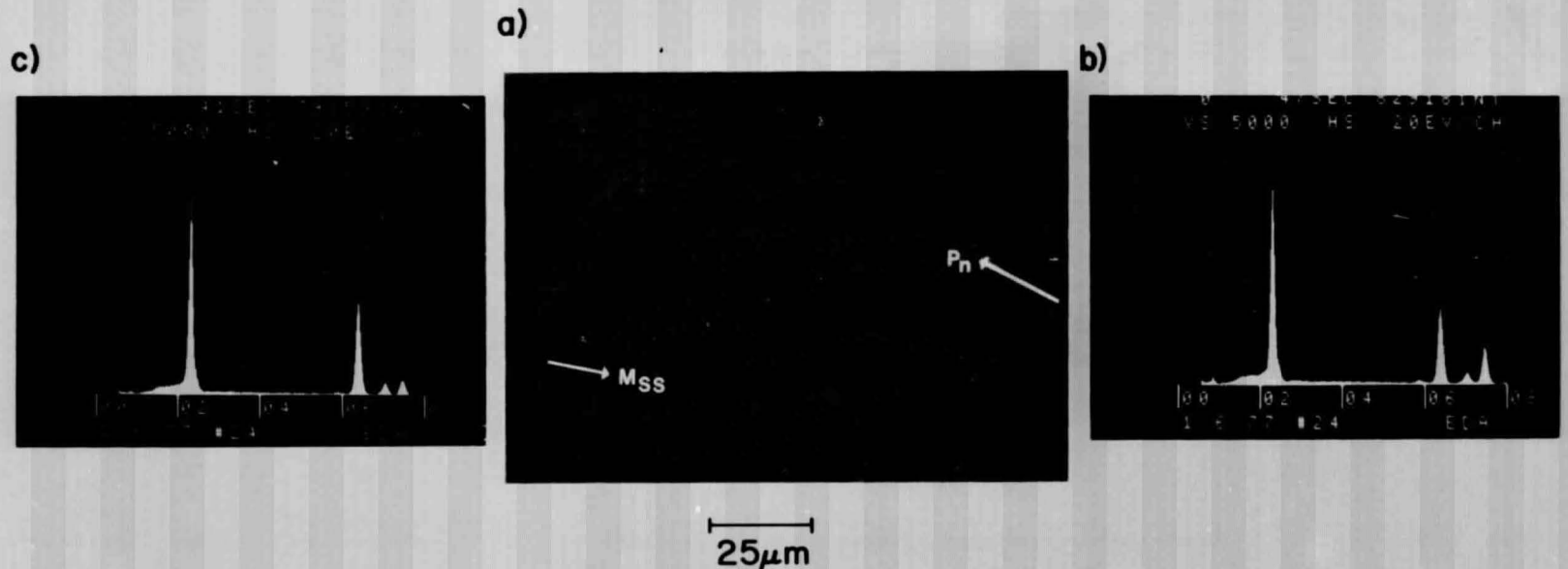

Fig. 6

Fig. 7

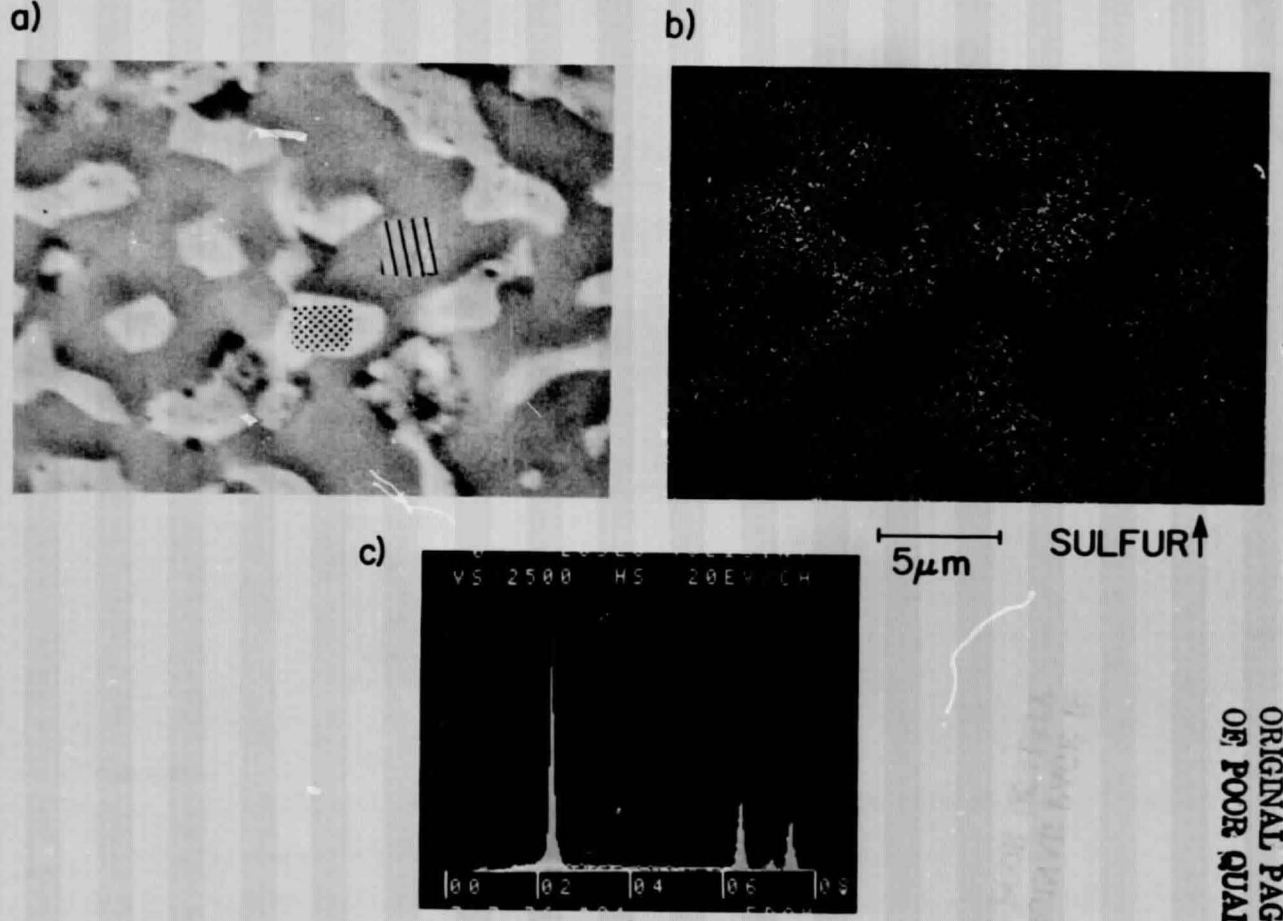

Fig. 8

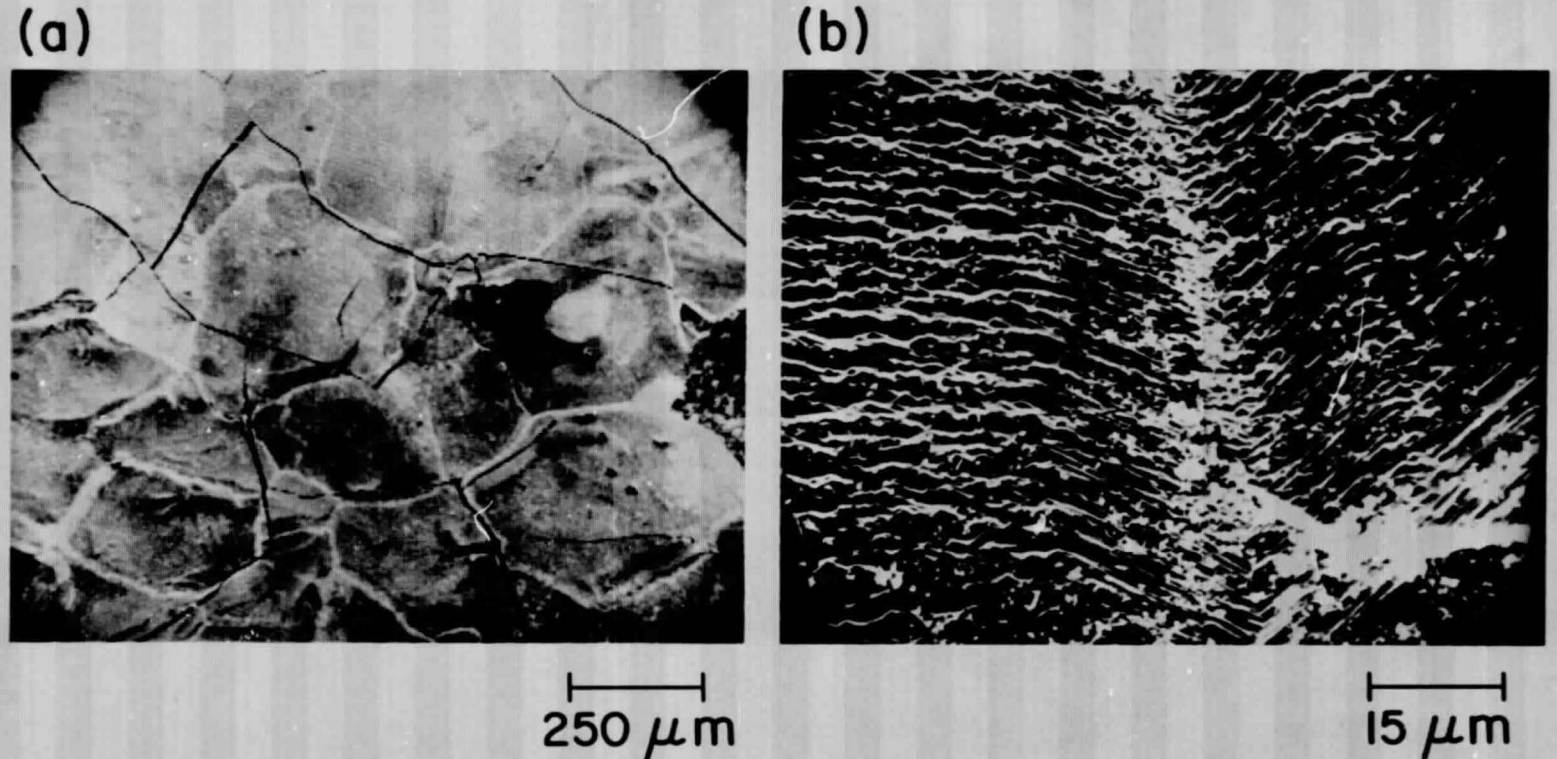

NASA-AMES
RAO

Fig. 9

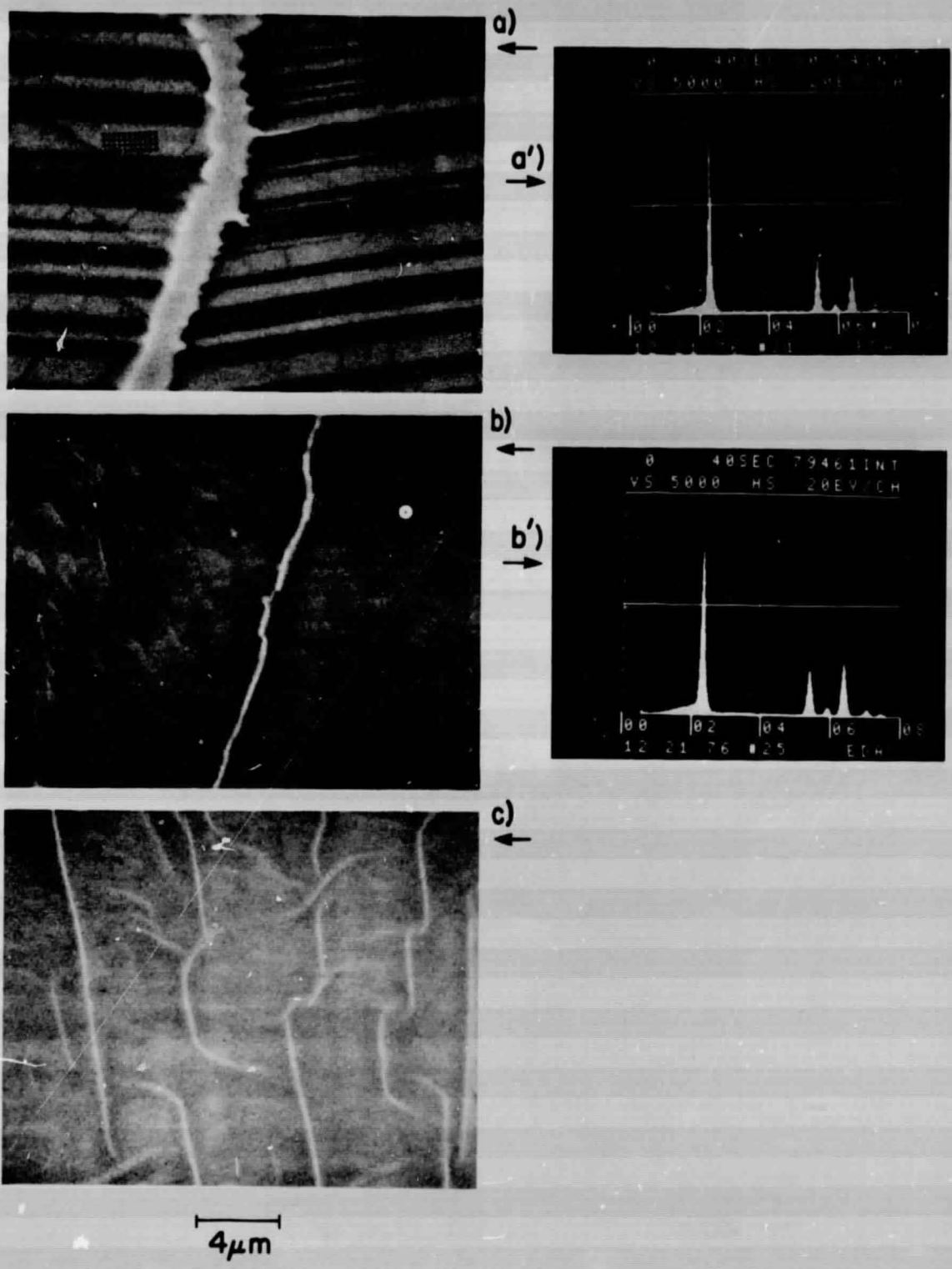

Fig. 10

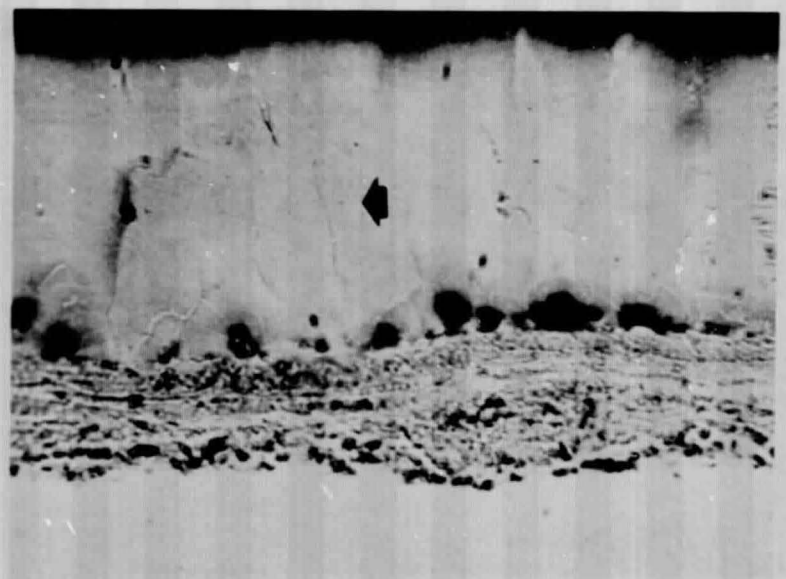

100 μm

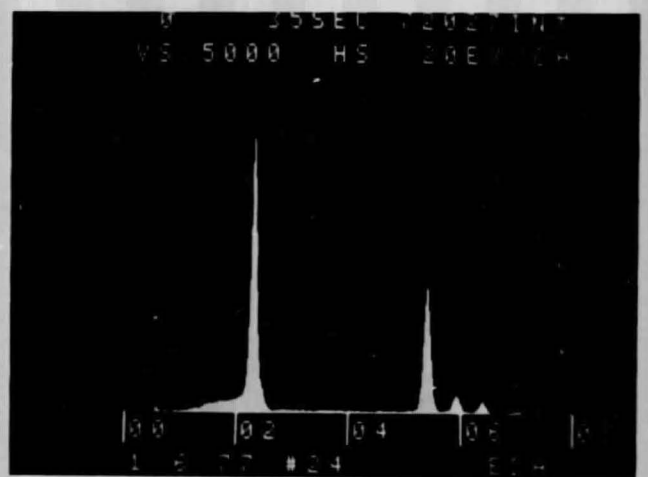

NASA-AMES
RAO

Fig. 11

a)

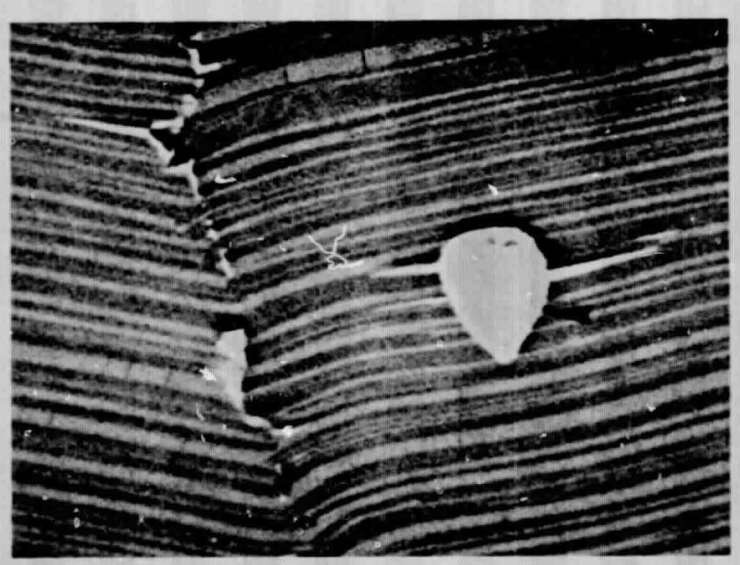

10μm

b)

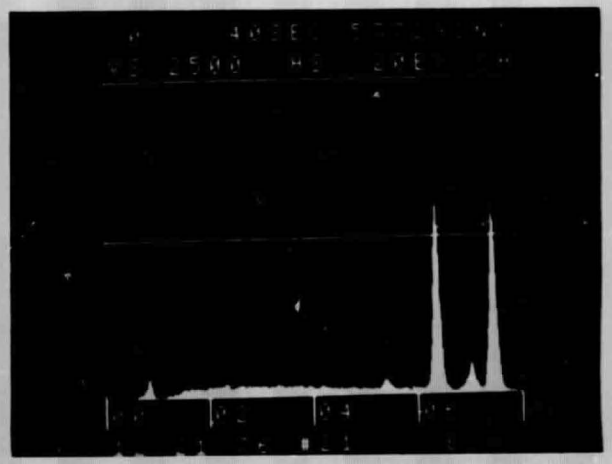

Fig. 12

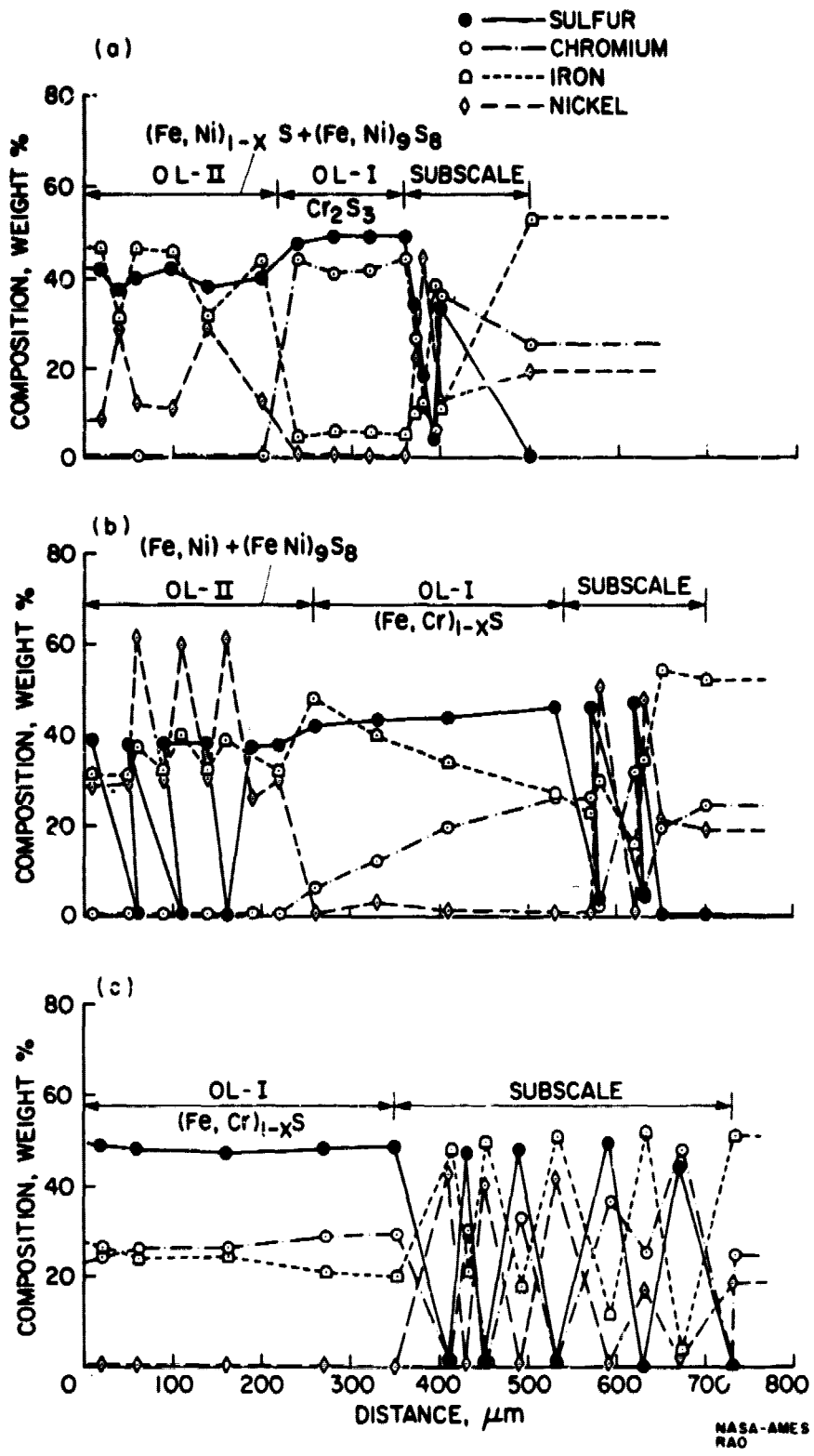

Fig. 13. Distribution profiles for iron, nickel, chromium and sulfur in the sulfide scales formed at a sulfur potential of 1.4×10^{-2} Nm^{-2}. (a) 933 K, (b) 1145 K and (c) 1280 K.

Fig. 14

NASA/AMES
RAO

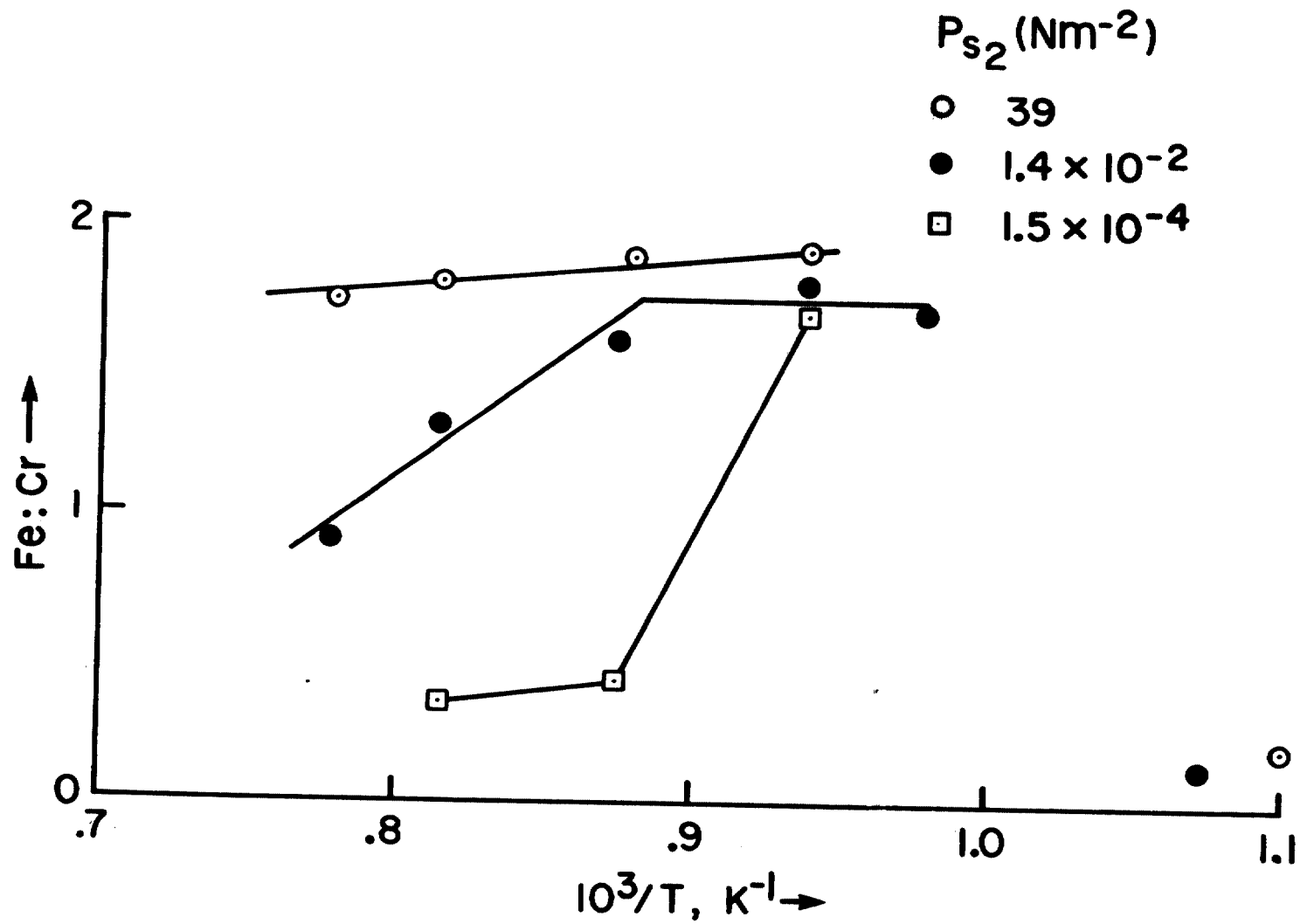

Fig. 15. Fe:Cr ratio of OL-I plotted as a function of the inverse of the absolute temperature.

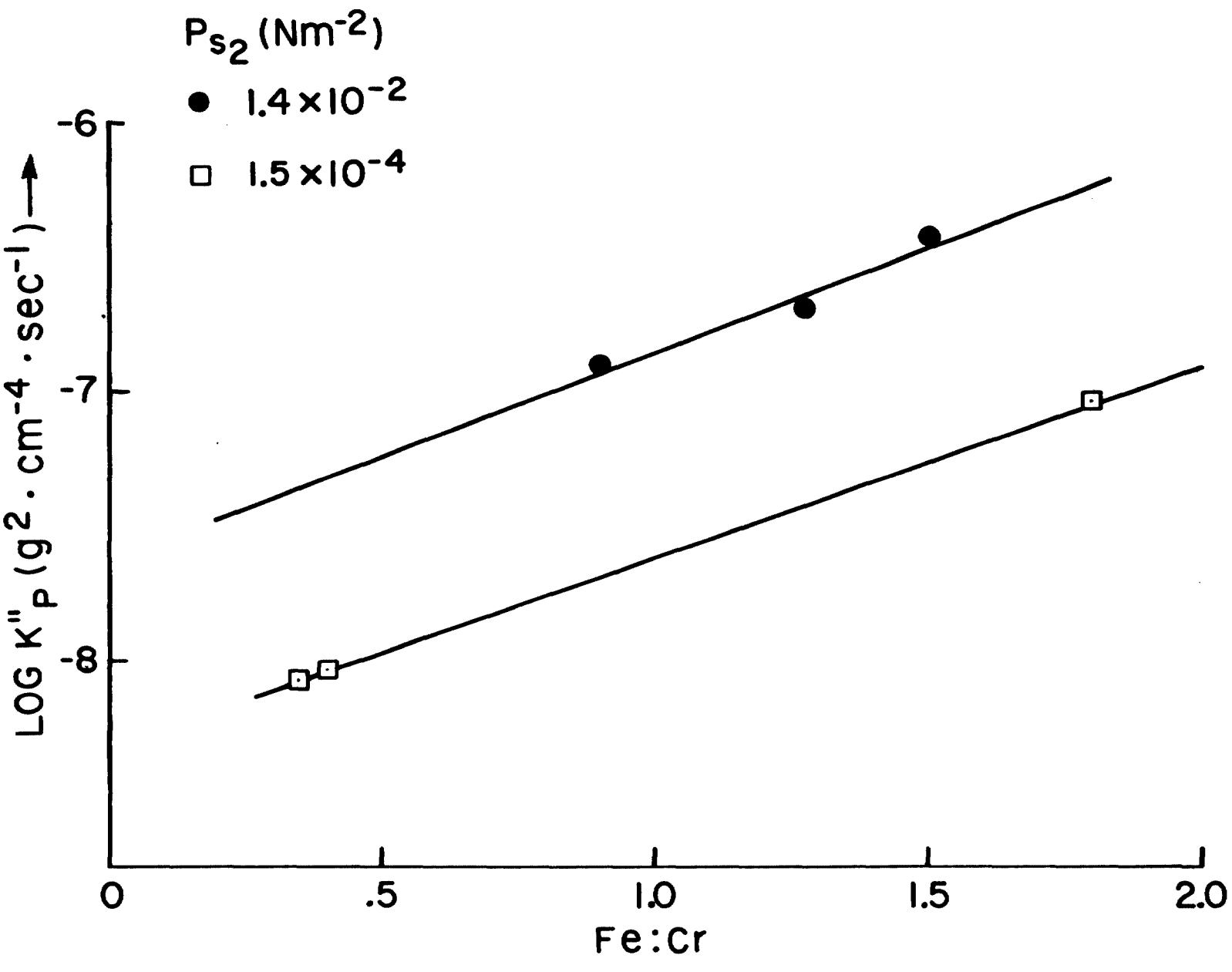

Fig. 16. The dependence of parabolic rate constants on the Fe:Cr ratio of OL-I.